Cement and Concrete Research 178 (2024) 107436

Contents lists available at ScienceDirect

Cement and Concrete Research

journal homepage: www.elsevier.com/locate/cemconres

Macro and microstructural evolution of low-calcium fly ash-based geopolymer mortar exposed to sulphuric acid corrosion

Piumika W. Ariyadasa [a], Allan C. Manalo [a,*], Weena Lokuge [b], Vasantha Aravinthan [c], Andreas Gerdes [d], Jonas Kaltenbach [d], Beatriz Arevalo Galvan [d]

[a] Centre for Future Materials, University of Southern Queensland, Toowoomba, 4350, QLD, Australia
[b] School of Engineering, Centre for Future Materials, University of Southern Queensland, Springfield, 4300, QLD, Australia
[c] School of Engineering, University of Southern Queensland, Toowoomba, 4350, QLD, Australia
[d] Institute for Functional Surfaces, Karlsruhe Institute of Technology, Karlsruhe, Germany

ARTICLE INFO

Keywords:
Low-calcium fly ash geopolymer
Laboratory-induced sewer corrosion
Acid neutralisation
Mass change
Microstructural evolution

ABSTRACT

This article reports an investigation of the behaviour of a low-calcium fly ash-only geopolymer (FAGP) mortar in comparison to Ordinary Portland Cement (OPC) mortar and a commercially available geospray mortar (P-GP) under laboratory-induced sewer conditions. An aggressive sewer condition was simulated by an accelerated corrosion rate, with mortar specimens immersed in 0.5pH sulphuric acid at a controlled temperature of 40 °C for 31 days. The macro and microstructural evolution of the specimens was analysed through visual observations, mass changes, and SEM coupled with EDS, XRD, and MIP analysis. OPC exhibited a 49 % mass loss attributed to the loss of the gypsum layer formed during the acid attack. The mass reduction in the low-calcium FAGP was only 6 %, which was 42 % lower than that of OPC, indicating that calcium-bearing hydrates in the cementitious binder systems are susceptible to sulphuric acid corrosion. The acid-resistant properties of FAGP mortar suggest its suitability for sewer rehabilitation applications.

1. Introduction

Geopolymers (GPs) are inorganic binders that are synthesised by mixing solid aluminosilicate precursors (from industrial waste), mostly fly ash (FA), ground granulated blast furnace slag (GGBFS), or metakaolin, with an alkali activator solution [1,2]. The polymerisation process begins and accelerates at higher temperatures when these compounds come together in the optimum concentrations [3]. Since GPs are clinker-free, their carbon footprint is up to 80 % lower than that of conventional Ordinary Portland Cement (OPC) [4]. These green binders offer an efficient waste management approach for the rise in manufacturing industries transitioning to a circular economy [5]. Therefore, GPs have been extensively researched as a potential binder material for various applications. Aside from being sustainable, alkali-activated geopolymers have piqued the interest of researchers as an alternative binder system to OPC due to their proven excellent mechanical properties and durability in aggressive environments [6–8]. GP performances are attributed to their three-dimensional Si-O-Al-O geopolymer network where amorphous alkali aluminosilicate hydrate, N-A-S-H (1) is the dominant gel phase [9,10]. This is different to the calcium silicate hydrate (C-S-H) gel in OPC matrices which is prone to acid-induced disintegration, as reported in Godinho and de Medeiros [11]. However, the characteristic of N-A-S-H gel bonds varies greatly depending on the ingredients used (type, dose of the amorphous precursor and alkali activators), mixing, compaction and curing, which change the gel structure and hence its macro behaviour [6]. The precursor oxides ratio for Ca/Al and Si/Al determines the two distinct GP subtypes, and the calcium-rich precursors, such as class C FA and slag varieties, produce strong calcium aluminosilicate hydrate, C-A-S-H (2) in addition to the highly cross-linked N-A-S-H bonds [5].

$$Na^{+} + SiO_2(OH)_2^{2-} \; or \; Si(OH)_3^{1-} + Al(OH)_4^{-} \rightarrow NASH \; gel \quad (1)$$

$$Ca^{2+} + SiO_2(OH)_2^{2-} \; or \; Si(OH)_3^{1-} + Al(OH)_4^{-} \rightarrow CASH \; gel \quad (2)$$

Nanopores are abundant in geopolymers and feature intricate pore architectures, making them lighter in weight than their OPC references [12]. The common assumption is that C(N)-A-S-H linkages have a positive effect on the calcium-rich geopolymers: they alter the pore

* Corresponding author.
E-mail address: allan.manalo@usq.edu.au (A.C. Manalo).

https://doi.org/10.1016/j.cemconres.2024.107436
Received 20 May 2023; Received in revised form 4 January 2024; Accepted 15 January 2024
Available online 29 January 2024

structure of the matrix into a cement-like form with higher mechanical strength than low-calcium geopolymers, making them suitable for various applications in the building and construction industry [13,14]. Wang et al. [15] documented that fly ash geopolymer paste with N-A-S-H gels is more porous and less dense than the slag systems with dominant C-(N)-A-S-H gels. Nonetheless, the effectiveness of calcium-rich geopolymers as a binder material is being challenged by some researchers [16,17] due to the drawbacks of rapid setting and increased drying shrinkage, which cause microcracking and are unfavourable to durability in severe conditions.

Literature [18–21] revealed that the calcium in geopolymers has a detrimental impact on the structural integrity when exposed to sulphuric acid. According to Nuaklong et al. [6] and Aiken et al. [22], exposure to sulphuric acid causes calcium cations (Ca^{2+}) to migrate from the geopolymer matrix and interact with the sulphate anion from the acid, producing gypsum deposited at the solid-solution interface. This soft, non-cohesive gypsum layer is acidic (pH < 2). It influences the pH of the surrounding concrete layer, attracting more sulphur-oxidising microbial species. This generates more acid to attack the inner layers of the matrix [23]. In this context, Grengg et al. [24] and Roghanian and Banthia [7] emphasised that special attention is needed when deploying geopolymers in sewer settings where there is a desperate need for acid-resistant and durable material against biogenic sulphuric acid to prevent or reduce substantial dissolution of portlandite from concrete and influence the alkalinity structure of the concrete pipe wall.

Ali et al. [25] revealed an increased focus on geopolymer research for applications in hostile sewer environments, which corresponds with the exponential growth in demand for concrete sewer rehabilitation. This is mainly due to the building and construction of new structures to accommodate increased population and urbanisation, human socio-economic and consumer patterns and climatic changes [26,27]. According to Zhang et al. [28], the lack of consistency in the outcomes of durability investigations is attributable to variations in the composition of the aluminosilicate precursor/s in the geopolymer and the acid exposure circumstances used. Since the natural sewer environment is a complex mixture of biological and chemical interactions, its circumstances might vary with location and time, making it difficult to compare data between studies and anticipate the geopolymer behaviour in natural sewers.

Matthieu et al. [18] evaluated the biogenic resistance of two cement-based linings made of calcium aluminate cement (CAC) with 29.4 % calcium oxide (CaO) and blast furnace slag cement (BFSC) with 42.8 % CaO, in laboratory-induced sewer conditions. Results confirmed the hypothesis that the calcium dissolution of the BFSC lining is higher than that of the CAC lining. In contrast to calcium-rich binder systems, where hydrates disintegrate quickly, CAC hydrates provide a longer chain of dissolution when subjected to acid attack, exhibiting significant acid neutralising capacity [23]. Opposed to this, Khan et al. [29] discovered that fly ash-based geopolymer (FAGP) lost an average of 0.4 % more mass after 12 months of field exposure in an aggressive natural sewer condition than alkali-activated slag-based mortar (AASm), in which the calcium content was approximately four times higher than FAGP. By comparing the pH of the exterior surface of initial and post-acidification and sulphur EDX mapping, they reported the neutralisation rate for AASm is lower than FAGP, concluding that decalcification of C-A-S-H does not necessarily impact the strength of the geopolymer matrix. In fact, it promotes the formation of N-A-S-H bonds in the absence of calcium. In another experiment, the same authors reported that calcium-rich sulphate-resisting OPC cement (SR) (59.7 CaO%) mortar showed higher mass loss compared to a calcium aluminate cement (36.5 CaO%) counterpart exposed to the same sewer condition. This disagreement could be attributed to the significant aluminium oxide (Al_2O_3) concentration in CAC compared to SR, as suggested by Lavigne et al. [21].

Considering all factors, chemically induced sewer conditions seem to be ideal in assessing geopolymer acid resistivity based on the available Ca content. Several researchers [10,18,30] discovered that the composition of CaO and Al_2O_3 in precursors directly impacts mass loss and acid neutralisation in the face of a sulphuric acid attack. The initial strength of the matrix is another crucial factor to consider when comparing acid resistance. The residual mechanical characteristics following acid exposure would provide an understanding of the vulnerability of a binder in sewer settings to predict the service life. Therefore, equivalent initial mechanical properties are vital for comparison. Comparing the efficiency against acid corrosion of the FA-based geopolymer to the Ca-rich equivalent is futile unless the initial strength is comparable. This is because FA-based geopolymers have more porous matrices, which promotes acid ingress into the interior layers, dissolving more ions regardless of their Ca content. However, this has not been considered in some experimental attempts, according to John et al. [8].

Nuaklong et al. [6] studied the durability of low-calcium FA (LCF) geopolymer mortar against extreme wastewater conditions (3 % H_2SO_4, pH of 0.3) for 84 days. Despite having the highest porosity and lowest compressive strength of all control mixes examined at 7, 28 and 90 days, they discovered that 100 % LCF had excellent resistance, with only 1.4 % weight loss and no visual deterioration compared to partial LCF mixes. Because no information on pore distributions and strength loss due to acid corrosion was documented, it was difficult to determine whether the pore structure of 100 % LCF was changed into one that was less permeable and thus positively affected, preventing acid ingress, or whether the phase changes that occurred at the acid attack were insignificant, resulting in no ion dissolution from N-A-S-H gels and no disintegration of the system by spalling off. Considering this, the effects of calcium content in the geopolymer matrix on acid-induced degradation, resultant pore structure and residual mechanical strength are inconclusive. As a result, for deploying low-calcium FA geopolymer as a protective layer in hostile sewage environments, more information is crucial on the correlation of GP phase shifts with variations in pore structure, mass and strength loss following acid exposure, necessitating future research.

The motivation to undertake this study, therefore, is to comparatively evaluate the performance of low-calcium fly ash binder systems and conventional OPC in a laboratory-simulated sewage environment. In the current study, the macro and microstructural evolution was investigated of low-calcium FA-based geopolymer mortar exposed to sulphuric acid corrosion. The phase changes in mortar systems due to acid attack were monitored using X-ray diffractometry (XRD), porosimetry, scanning electron microscopy with energy dispersive X-ray spectrometer (SEM-EDS) and element mapping, which assisted in identifying the deterioration that occurred. The results given in this study will support materials developers and design engineers in optimising repair binder systems with Ca-deficient source materials and predicting the degradation behaviours in actual sewer conditions.

2. Materials and methods

2.1. Mortar specimens

This study comprised of mainly two mortar types: fly ash-based alkali-activated geopolymer (FAGP) and OPC. Class F fly ash (sourced from Gladstone Power Station, Queensland, Australia) was employed as the single aluminosilicate source from which to manufacture FAGP mortar. Its chemical composition, as obtained from an X-ray fluorescence (XRF) examination, is shown in Table S1 (Appendix). This study includes a proprietary geopolymer (P-GP) spray mortar to benchmark the initial strength target and to compare mass loss owing to acid deterioration. However, for confidentiality, XRF results of P-GP cannot be shared. P-GP mortar was produced by adding potable water to the one-part binder mix according to the product specifications. As shown in Table 1, the mix composition for FAGP and OPC mortars was chosen to attain equivalent mechanical strength with P-GP, which is 40 MPa compressive strength.

A 1:2 combination of sodium hydroxide (16 molarity NaOH) and

Table 1
Mix composition of mortar specimen.

Mix ID	FAGP	OPC	P-GP
	(kg/m^3)	(kg/m^3)	(kg/m^3)
Fly ash (FA)	396	–	–
Ordinary Portland Cement (OPC)	–	370	–
Proprietary geopolymer spray mortar Binder (P-GP)	–	–	796[a]
Fine aggregate	754	555	–
16 M Sodium hydroxide solution (NaOH)	85	–	–
Sodium silicate solution (Na_2SiO_3)	170	–	–
Extra potable water	0.8	166	103
Liquid/binder (L/b)	0.32	0.45	0.13
Alkali activator solution/ binder (AAS/b)	0.55	–	–
Na_2SiO_3/NaOH	2	–	–
Curing condition	24 h @ 80 °C 27 days @ 24 °C	28 days @ 26 °C, 86 % RH	28 days @ 26 °C, 86 % RH
Density (kg/m^3)	2028	2203	2144
28- day compressive strength (MPa)	41.9 ± 2.7	45.0 ± 2.4	40.8 ± 1.4

[a] Inclusive of binder and aggregates; RH- Relative humidity.

sodium silicate solutions activated the FA. Several researchers [31,32] have proposed keeping this alkali activator solution (AAS) for 24 h before combining it with FA so as the exothermic reaction subsides. The mass ratio for the activator solution to binder was 0.55 while the liquid-to-binder ratio was maintained at 0.32. Both FAGP and OPC mortars were prepared using river sand as the fine aggregate at a ratio of 1.5 to the binder weight. Cylindrical mortar specimens were 30 mm in diameter and 30 mm in height and were cured at different temperatures (Table 1) for 28 days; the curing conditions chosen were based on previous research suggestions [33]. Due to confidentiality, the chemical composition of the binder material or related corrosion product specifics of P-GP are not published in this work.

2.2. Exposure conditions

Available studies [34] suggested that reproducing the circumstances and interactions in natural sewer environments is difficult due to their complexity and lengthy processes. In comparison studies for concrete corrosion, microbiological testing is more degrading than chemical tests. As there is currently no standard procedure for simulating aggressive sewer conditions, similar approaches implemented in previous studies were adopted. Some researchers have attempted to recreate natural sewer conditions through an accelerated laboratory experimental condition that uses either H_2S (ppm) or the pH level with the relative humidity (RH) of the aggressive sewer conditions. 5 ppm $< H_2S <$ 400 ppm [24,34] or $<$ 1 pH level of the sulphuric acid medium with an RH of at least 98 % (i.e. temp. $>$ 30 °C) are commonly reported values [35,36].

Table S2 (Appendix) outlines experimental attempts with sulphuric acid to model microbial-induced concrete corrosion, which provided a basis for the approach implemented in this study. According to Table S2 (Appendix), sulphuric acid with a pH of 0.5 to 1.0 was typically employed to achieve the natural sewer condition. Other than the pH level or the acid concentration, acid volume per specimen, and exposure duration appear to be major determinants in deterioration [15].

Considering the above, an accelerated laboratory chemical degradation process was deployed in this study, with the pH of sulphuric acid controlled at 0.5 to replicate aggressive sewer conditions. Three replicates of specimens for each mortar type were used for sulphuric acid testing. In accordance with the acid corrosion testing protocol used by Khan et al. [29], mortar specimens were precisely measured for diameter and weight, and then plunged into identical chambers filled with the sulphuric acid solution at a liquid-to-sample volume ratio of 4.5. Specimen chambers were kept in an incubator at 40 °C, as recommended by Grengg et al. [37] and Wells and Melchers [38] to facilitate the desired RH. The acid solution in the specimen chamber was set to agitate at a speed of 30 rpm to ensure homogenic contact with acid mimicking the condition in a typical sewer pipe. The acid solutions were replenished when pH reached 1, otherwise, weekly.

2.3. Sampling and analysis

2.3.1. Variation in acid solution pH

The pH of the exposure solution (H_2SO_4 acid) was periodically monitored to ensure stability at a constant value of 0.5 ± 0.1; the pH measurements were obtained using a calibrated benchtop pH meter. The assessment of acid consumption behaviour in different mortar types involved quantifying the rate of pH variation during each pH adjustment period.

2.3.2. Mass variation

The mass change of samples was determined using Eq. (3) based on ASTM C267-20, where δm (%) is the total mass change measured after the acid exposure and *mi* and *mc* are the initial mass and mass after acid exposure, respectively. The data used in this calculation was an average of three samples. Before weighing, the acid-soaked specimens were washed thoroughly to free them from loose particles and then dried in an oven at 60 °C for minimum 24 h [39] until no change in mass was observed.

$$\delta \mathrm{m} = (mc - mi) \times 100\%/mi \tag{3}$$

2.3.3. Microscopy analysis

Microstructure evolution was assessed in mortars using a TESCAN VEGA 111 scanning electron microscope (SEM) with an accelerating voltage of 25 keV. A full-sized sample was studied for microstructure over the slice width with a low vacuum SEM. This allowed sensitive specimens, such as the extensively spalled OPC, to avoid further damage from fracturing into a smaller-sized SEM sample. Aside from examining a specific region of interest, the stitching capability of the TESCAN VEGA 111 scanning electron microscope enabled the partition of the entire sample area into discrete working sections, magnification of each segment and subsequent seamless integration of these sections. The benefits of this technology include the ability to perform quick spot inspections, detect microstructural changes across a given length of an object and ensure data retention for future use.

2.3.4. X-Ray Diffraction Analysis

XRD was used to evaluate the phase alterations of FAGP and OPC mortars caused by acid exposure. Spectra were acquired for representative powdered samples from the degraded zone and the sound core using a D8 Advance Bruker diffractometer configured for 40 kV, 40 mA and Cu K radiation. The DIFFRAC.EVA program with an inbuilt comprehensive global library of spectral patterns was used to analyse data and identify the crystalline and amorphous phases.

2.4. Elemental mapping

The spatial distribution of elements in deteriorated mortar samples was studied using a VEGA 111 X-ray energy dispersive spectroscopy (EDS). Maps of several elements over the same area were created to characterise the phase changes. This method facilitated a qualitative comparison of phases at the damaged zone with the sound core. Due to its non-destructive nature, the EDS technique enables the analysis of significantly damaged specimens without sample pre-treatment.

2.4.1. Mercury Intrusion Porosimetry (MIP)

A fully automated Pasca 440EVO porosimeter was used to quantitatively analyse porosity changes in mortar specimens before and after acid exposure. Samples from the deteriorated exterior and the unexposed core were placed into the MIP for vacuum-assisted degassing in preparation for pore analysis. The pore size was calculated in MIP analysis using the Washburn eq. (4), which accounts for the applied pressure and the associated cumulative intruded mercury volume.

$$D = -4\delta cos\theta / P \quad (4)$$

where D is the pore diameter (μm), P the applied pressure (N/mm^2), θ is the contact angle between mercury and the pore wall (140°) and δ the surface tension of mercury (0.48 N/m).

3. Results and discussion

3.1. Variation in acid solution pH

Fig. S1(a) (Appendix) illustrates the acid-immersed mortar specimens housed inside the incubator at a controlled environment of 40 °C and a shaking speed of 30 rpm. The results depicted in Fig. 1 are the observed pH variation of the acid solutions, with each data point being the average of the pH readings of three samples. The inspection of mortar specimens after 31 days of acid exposure indicates the influence of the pH and temperature of the acid solution on matrix disintegration. The pH level of the acid solution changed for all mortar types, although at varying rates during the exposure duration, indicating that the mortar matrices have varying buffering capacities. As illustrated in Fig. 1, FAGP experienced a pH change from 0.5 to 1.11 on the seventh day of acid exposure, indicating a faster start of the neutralising process than OPC and P-GP, which only scaled up to pH 1.05 and 0.97, respectively. Nevertheless, further monitoring revealed a noticeable reduction in the change of solution pH for FAGP, suggesting a relatively slower rate of acid neutralisation than OPC and P-GP. The pH fluctuations observed in all types of mortar during the study exhibit a similar trend, characterised by a decrease in the rate of change over time, as shown in Fig. 1. Fig. 2 depicts an overview of the weekly fluctuations in the pH levels recorded for each mortar sample.

Fig. 2 illustrates that, compared to OPC and P-GP, the acid neutralisation rate of FAGP sharply decreases between Weeks 2 and 3. However, OPC appears to sustain a consistent reduction in acid neutralising capacity. This phenomenon can be attributed to the dual processes of ion dissolution that occur when a geopolymer is exposed to a strong sulphuric acid solution with a pH below 2.0, as described by Pather et al. [40]. The initial stage involves liberating Al ions from the silicon-oxygen-aluminium (Si-O-Al) bonds in the geopolymer matrix, neutralising the acidic pH level. Subsequently, Ca^{2+} ions are exchanged from the

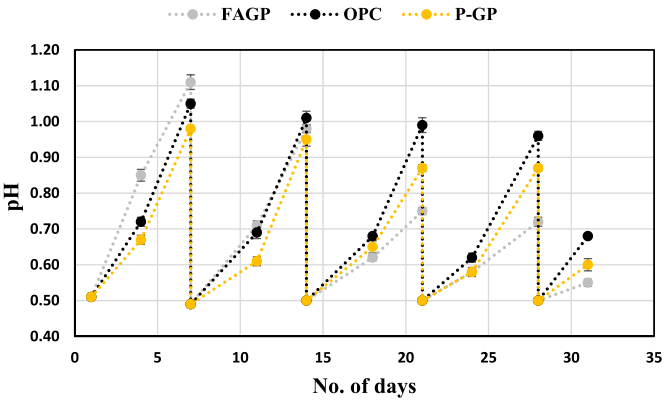

Fig. 1. Variation in pH levels of the sulphuric acid solutions during the study period.

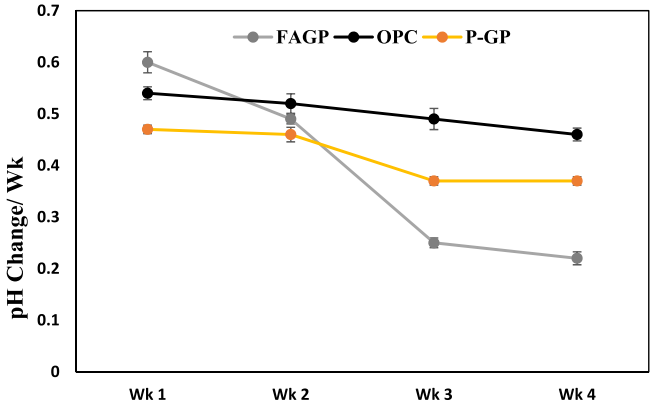

Fig. 2. The behaviour of acid neutralisation of each mortar during the study period.

geopolymer gel with sulphate anions from the acid. If no Ca^{2+} exists in the geopolymer matrix to dissolve, the acid neutralisation process is impeded. During a sulphuric acid attack, Ca^{2+} ions are the first to be released from cement hydrates, followed by aluminium and ferric oxide hydrogels, which depend on the pH of the acid solution [23]. Because aluminium hydrogels dissolve at pH values <3 [41], there is a strong possibility of dissolving and leaching aluminium ions from hydrogels in the 0.5 pH acid media used in this study. The percentage of Al^{3+} ions in OPC is, however, low compared to Ca^{2+}; the leachate is believed to be primarily Ca^{2+} ions and these ions seem to be continuously forming $CaSO_4$ by breaking $SO4^{2-}$ from the sulphuric acid solution.

It is evident from Fig. 2 that P-GP leachate had the least effect on the acid solution pH of all three mortar types during the first two weeks of exposure; the pH change rate per week remained consistent. However, this decreased (from pH level 0.46 to 0.37) in Week 3; nonetheless, the change was not significant compared to FAGP. Even though the acid solution was replenished to maintain the acid concentration, the pH shift for all mortar types appeared stable between Weeks 3 and 4, indicating a slower exchange of ions between the matrix and the acid. FAGP had the lowest acid neutralising rate during the final phase of exposure, followed by P-GP. As expected, OPC demonstrated the highest pH buffering capability, which previous researchers attributed to the continual release of Ca^{2+} ions from C-S-H linkages of the cementitious matrix.

The acid neutralisation process can also be influenced by a possible H^+/OH^- balance in the system if not replenished. This is unusual in natural sewer circumstances, in which the sulphur-rich wastewater flow feeds the microbial species to generate more sulphuric acid. According to Khan et al. [39] and Monteny et al. [42], a chemically-induced degradation test has a lower corrosion rate than a microbiologically induced test because the porous corrosion layer in sewers creates bacterial growth, while the corrosion products from the chemical test act as a barrier, reducing acid diffusion to the sound matrix. This behaviour was not observed in this study. This is attributed to the removal of unstable gypsum at a pH value <1 when the solution was stirred, allowing acid to contact the sound matrix, which is typical in natural sewer settings. Also, the periodic replenishment of acid solution aided in maintaining the reaction momentum.

3.2. Visual observation and mass changes

Fig. S1(b) (Appendix) illustrates the visual change observed in the three types of mortars following a 31-day immersion in 0.5 pH sulphuric acid at 40 °C, replicating harsh sewer conditions. Fig. S1(b) shows OPC specimens before and after being subjected to the sulphuric acid. The changes in OPC specimens were instant after being exposed, and within three days, they began to deteriorate, and sediment accumulated around them. The OPC specimens showed substantial dissolving of solid

material, resulting in severe surface disintegration. OPC decreased in diameter from 29.9 mm to 20.5 mm on average for the three samples, representing a 48.7 % material loss (Table 2). This observation was consistent for all three samples. This differs from the findings of Albitar et al. [43] who observed a 1 % mass gain for OPC after 30 days of exposure to 3 % (0.8 pH) sulphuric acid. This can be attributed to the higher concentration of acid (3.4 %, 0.5 pH) and increased temperatures (40 °C) used in the present study, which may have accelerated the degradation process and obscured the slight increase in the OPC mass. Another factor that can contribute to this discrepancy is the acid solution to sample surface area ratio; however, no information is available to correlate this with the change in mass. The white soft foamy layer seen at the OPC surface was identified as gypsum which resulted from the reaction between calcium hydroxide (portlandite) and sulphuric acid. The brown coloured ring between the gypsum and the OPC inner core is referred as the margin of the acid penetration depth.

Fig. S1(b) reveals that the degree of damage observed in FAGP specimens after acid immersion was not significant. The colour slightly faded, and the diameter loss after 31 days was only approximately 1 mm. In terms of mass loss, this is 42 % lower than OPC, which aligns with the findings of Khan et al. [44]. They observed that fly ash-based geopolymer mortar (FAGP), composed of 80 % fly ash (FA) and 20 % ground granulated blast furnace slag (GGBFS), deteriorated at half the rate of sulphate-resistant Portland cement mortar (SRPCm) when exposed to a pH 1 sulphuric acid solution for a duration of 8 weeks. For FAGP (Fig. S2b), a noticeable colour difference can be seen between the three zones: the deteriorated, semi-deteriorated and sound core. This is due to the acid penetration, chemical interactions with matrix and ion dissolution followed by the acid attack.

The FAGP semi-deteriorated or transition zone can be seen via the brown coloured ring approximately 5 mm from the outer surface, indicating the penetration depth and region up to which the matrix is impaired. Like in OPC, the outer surface of the P-GP mortar specimens (seen in Fig. S1(b)) was coated with soft white pulpy substance; however, the thickness was less than the OPC's, and the surface disintegration in mass loss was approximately 11 %. The colour change in the acid solution was also noted to differ across the mortar types, with the OPC having a white colour from the dissolved gypsum. FAGP had a greenish tint, which can be attributed to probable Al or Si dissolution from the matrix. The brown colour of the P-GP acid solution is assumed to be from basalt fibres [45] or another unknown substance from the binder mix that was attacked by sulphuric acid. After acid exposure, P-GP exhibited the roughest surface of the three mortar types. This can be attributable to the bigger aggregates employed in the mix (1–4 mm in size) which have been exposed due to the deterioration of the matrix's outer layer. The surface roughness of OPC and FAGP was minimal when compared to P-GP. This could be due to the usage of fine aggregate in manufacturing OPC and FAGP with a maximum grain size of 1.18 mm. The acid degradation and consequent surface roughness can be affected by the size and type of aggregate used [40]. Further tests are recommended to evaluate the effect of the nature of aggregates on the surface roughness induced by acid attack.

Table 2
Mortar specimen dimensions after acid exposure.

Mortar type	Before acid exposure		After acid exposure			
	Avg. dia (mm)	Avg. mass (g)	Avg. dia. (mm)	Avg. % dia. loss	Avg. mass (g)	Avg. %
FAGP	29.7 ± 0.08	43.6 ± 0.07	29.1 ± 0.21	1.91 ± 0.83	40.8 ± 0.33	6.4 ± 0.66
OPC	29.9 ± 0.17	47.8 ± 0.02	20.5 ± 0.37	31.2 ± 1.52	24.5 ± 0.58	48.7 ± 1.23
P-GP	30.2 ± 0.21	46.3 ± 0.06	27.4 ± 0.54	9.4 ± 2.04	41.2 ± 1.04	11.0 ± 2.19

3.3. Microscopy

Representative SEM images with different magnifications were used to depict the morphological evolution of the deteriorated OPC and FAGP mortar samples following the acid attack. Fig. 3(a) depicts a micrograph of a deteriorated OPC specimen (sliced at a depth of 5 mm from the surface) captured from a TESCAN VEGA 111 SEM model; this micrograph is a compilation of individual micrographs taken at x109 magnification and stitched. Figs. 3(b) and 3(c) represent selected areas from the core and deteriorated outer zone, respectively. Figs. 3(d) and 3(e) are the magnified versions of micrographs 3(b) and 3(c). Fig. 3(d) reveals the formation of ettringite: a primary reaction product is formed in the hydrated OPC system as a result of gypsum reacting with tricalcium aluminate (C_3A). This indicates that acid infiltration has progressed beyond the visible damaged outer zone and is reacting with the sound matrix. Fig. 3(e) shows the formation of obvious expansive gypsum fracturing the binding between the fine aggregate and the OPC binder, resulting in fissures that eventually aid in the spalling of the corrosion products.

Fig. 4 displays the corresponding EDS graphs (as an average of the highlighted locations), where 4(a) and 4(b) represent SEM micrographs acquired at the OPC core and outer deteriorated zone, respectively. When comparing the corresponding EDS graphs of Fig. 4(a) and 4(b), peak intensities for Si, Ca, and S shift significantly, demonstrating the different microstructural arrangements across the OPC sample, with more sulphur localised at the deteriorated zone. On the contrary, Table S3 (Appendix) shows that the OPC core area, as shown in Fig. 4(a), had lower S but higher Ca, Al and Si percentages which promote highly expansive ettringite in the presence of acid attack. These findings correspond to the morphological changes noted above between the substantially disintegrating OPC matrix and the exposed but not visibly damaged matrix. Microcracks are evident in the core zone and must result from the quick setting of fresh OPC mortar during the hydration process. The microcracks in the degraded zone, on the other hand, are a direct outcome of the formation of expansive gypsum.

Fig. 5 depicts the micrographs of deteriorated FAGP specimen. Fig. 5 (a) exhibits a collection of individual micrographs representing the middle layer of an FAGP specimen exposed to 0.5 pH sulphuric acid for 31 days. Fig. 5(b) exhibits a SEM image of the magnified area of the transition zone, which is the brown ring depicting the depth of acid penetration in the FAGP matrix. When further magnified, Fig. 5(c) shows that the aggregates and geopolymer binder in this zone are still intact, with no noticeable disintegration at the binder aggregate interfacial transition zone (ITZ). However, a wide spread of bright white particles is visible in this zone, each with a circular form and varying sizes (see Fig. 5d). This can be attributed to the Fe^{3+} ions migrated and precipitated at the acid front. The EDS results shown in Fig. S2 (Appendix) to support this. Similarly, a SEM analysis was performed on the deteriorated outer zone of the FAGP sample and is depicted by Fig. 5(e). A distinct colour change in the matrix from dark grey to pale grey occurred, following the acid attack. This can be linked to the matrix neutralisation process which occurs when the mortar matrix leaches ions while consuming H^+ from the acid solution.

The aggregate particles were dispersed, as seen in the SEM micrograph in Fig. 5(e). Still, they did not exhibit the significant cracking observed in the deteriorated zone of the OPC sample (Fig. 5(b)). According to Khan et al. [44], this is caused by removal of Ca^{2+}, Na^{1+} and Al^{3+} from the matrix near the exposure zone as a result of decalcification, loss of alkali and dealumination. They reported the highest concentration of Na and Al ions leaching out from FA geopolymer mortar within the first week of sulphuric acid exposure, compared to the cement-based mortar which had the highest Ca ion removal. As Fig. 5(f) shows, the FAGP mortar matrix experienced microcrack propagation between the aggregate and geopolymer matrix due to the formation of secondary phases with Na and Al deficient polymeric linkages. A selected area from Fig. 5(f) that represents the geopolymer binder is

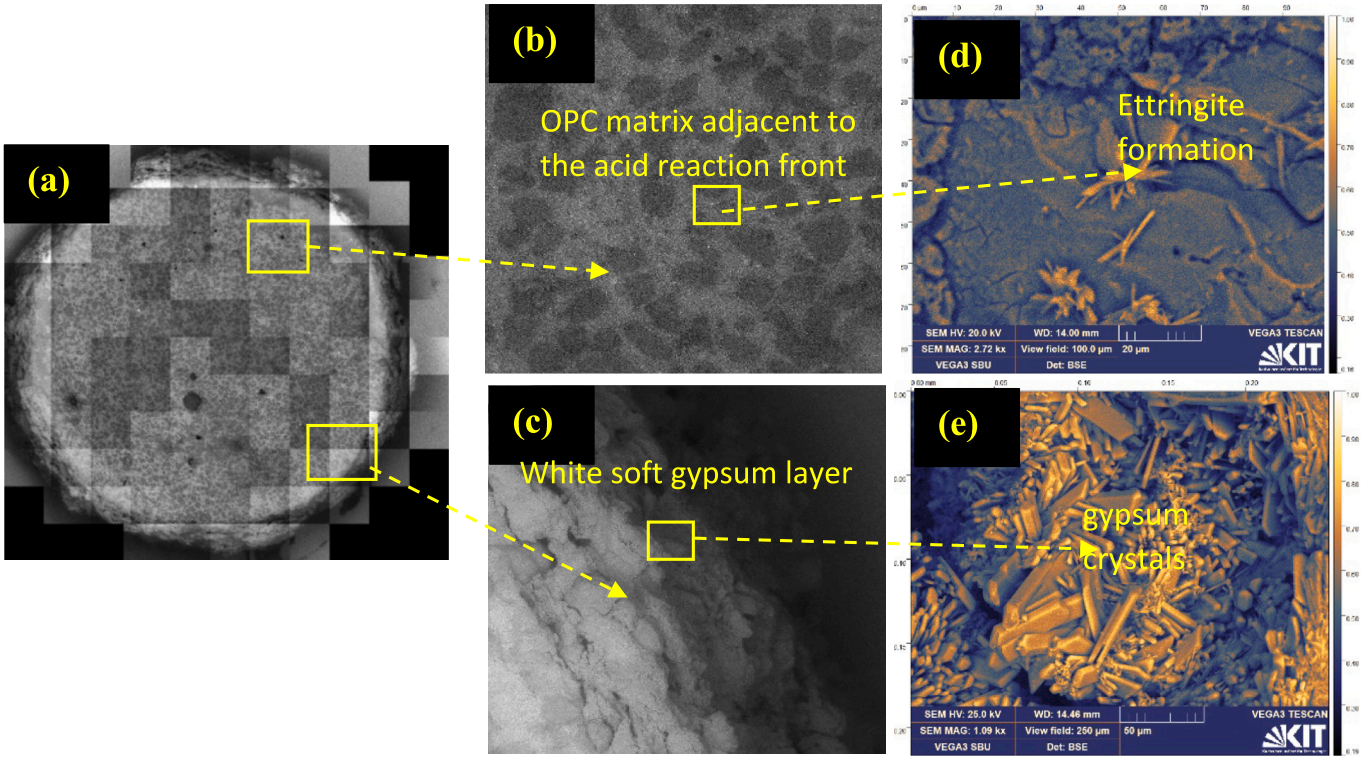

Fig. 3. OPC mortar sample, (a) stitched SEM micrograph, (b) magnified matrix adjacent to the acid reaction front, (c) deteriorated outer zone, (d) and (e) are further magnified images of (b) and (c), respectively. (Note: Figs. 3(d) and 3(e) are enhanced with distinct colours using Gwyddion 2.53 software for easy recognition of the phase transition; the colour index based on the intensities of the original image is shown on the right side of the image.)

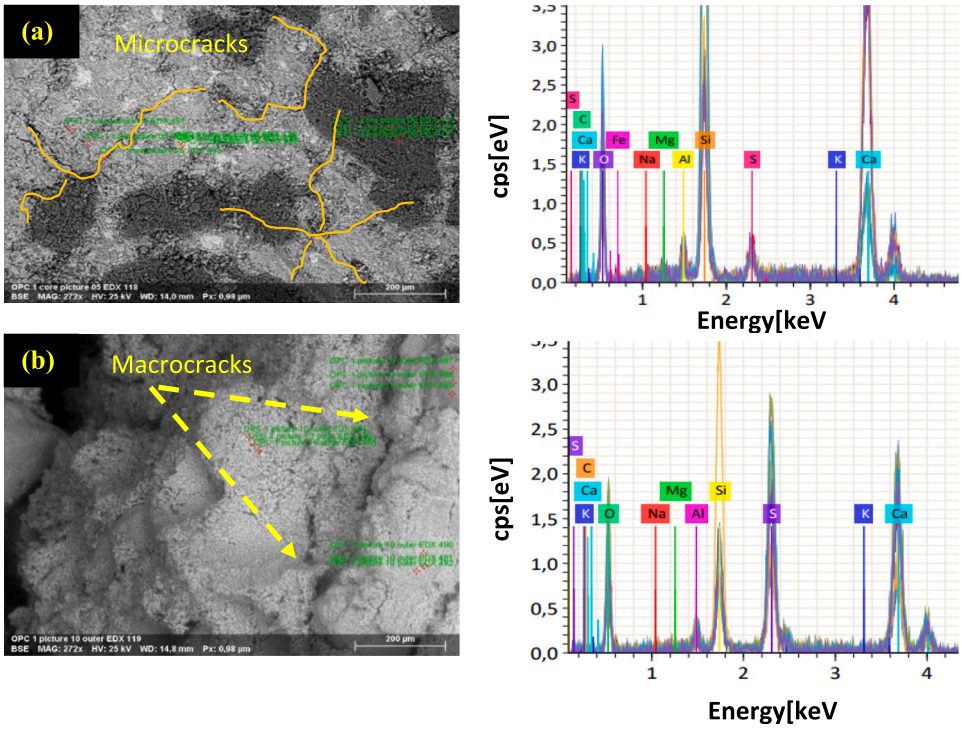

Fig. 4. SEM images with EDS elemental mapping of OPC (a) core and (b) deteriorated zone (as an average of the marked points).

magnified to investigate the microstructure of possible secondary phases or corrosion products. Fig. 5(g) indicates an abundance of microcracks in the matrix; however, no evidence for the existence of either gypsum or ettringite can be found.

Fig. S2 (Appendix) summarises the EDS analyses performed at various locations of the FAGP mortar specimen, namely the FAGP core, the bright particle encountered in the semi-deteriorated (brown ring), and the deteriorated outer zone, which are labelled as 1, 2, and 3

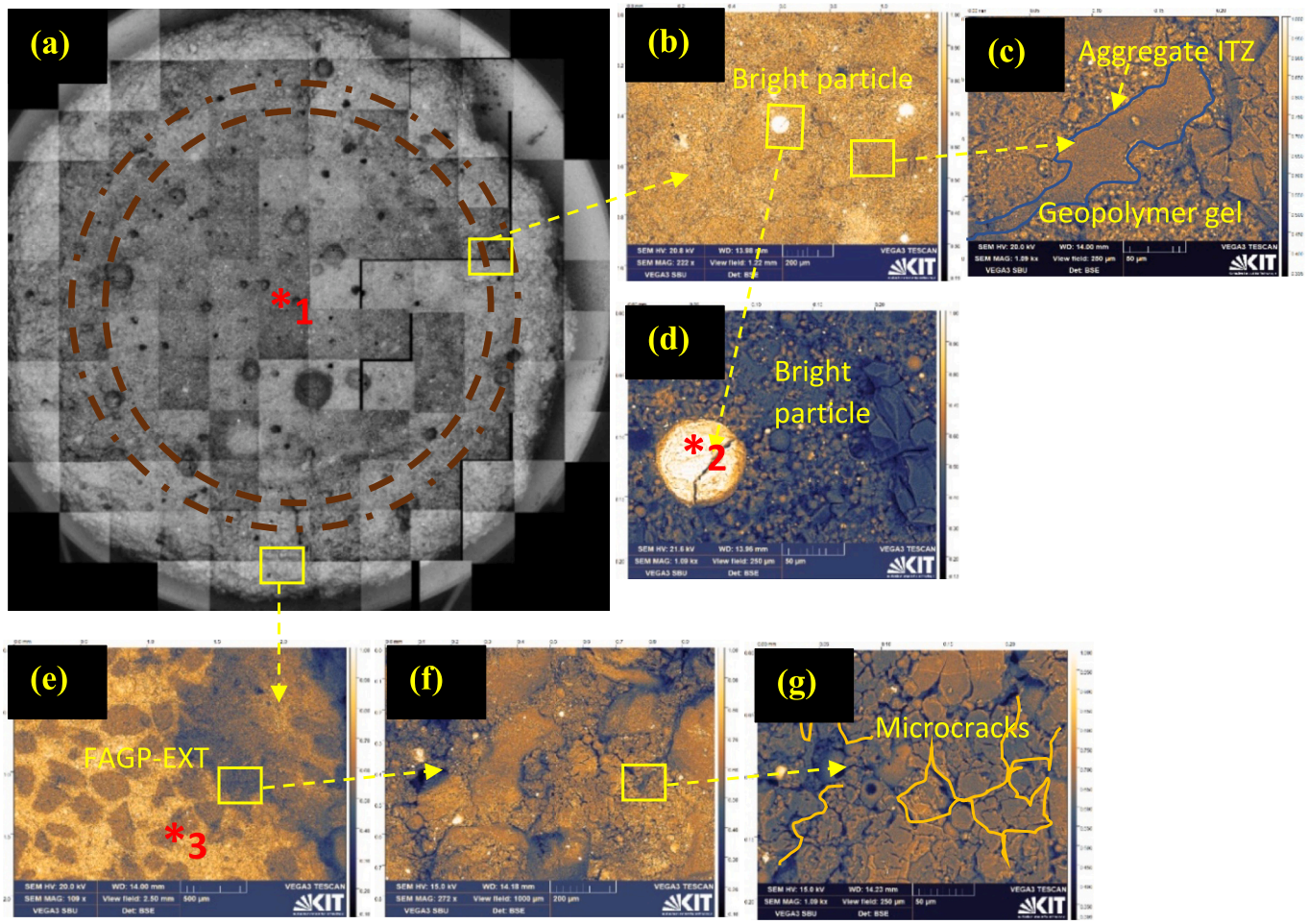

Fig. 5. FAGP mortar sample (a) stitched SEM micrograph (b) transition zone, (c) magnified area of (b), (d) magnified area of bright particle. (e), (f) and (g) SEM graphs for deteriorated outer zone at various magnifications. Note: Figs. 5(b) to 5(g) are enhanced with distinct colours using Gwyddion 2.53 software for easy recognition of the phase transition; the colour index based on the intensities of the original image is shown on the right side of the image.

respectively in Fig. 5. Each area of concern is based on a three-point average. The atomic concentration of metal cations appeared to be lower in the degraded zone compared to the FAGP core, confirming the probable leach-out into the acid solution. The concentrations of Al and Na ions removed from the deteriorated area of matrix in leachate were computed to be around 70 % and 85 %, respectively. Khan et al. [44] observed a similar scenario in which the acid neutralisation potential of geopolymer mortar was reduced at the end of the initial phase of the experiment because of Na^{1+} and Al^{3+} ions already being removed from the matrix near the exposure surface due to alkali loss and dealumination. After 14 days of exposure, they reported 712 mg/L and 2580 mg/L leachate concentrations of Al and Na following FA geopolymer specimens. The calcium ion concentration in the FAGP core (Fig. S2 (Appendix)) appeared to be insignificant in comparison to the deteriorated zone, confirming the absence of gypsum or ettringite formations in the SEM pictures (discussed previously) of the deteriorated zone. The presence of sulphur is only visible in the degraded zones, showing that SO_4^{2-} was transferred into the matrix during the neutralisation of H^+ ions. Interestingly, Fe ion concentration appeared to be higher in the semi-deteriorated zone compared to the rest of the FAGP specimen regions, which can be attributed to the dissolution of reactive Al^{3+}, allowing Fe^{2+} ions to agglomerate at the transition zone. This is discussed further below.

3.4. X-ray diffraction analysis

XRD analysis was performed on mortar specimens after 31 days of exposure to 0.5pH sulphuric acid. The XRD spectra of FAGP and OPC are shown in Fig. 6 and Fig. 7, respectively. The exposed specimens were compared with the reference sample for each mortar type, denoted as the control sample. This approach can verify the presence of emerging new phases at the deteriorated (Exposed EXT) and semi-deteriorated (Exposed INT) zones compared to the undeteriorated core (INT) at the exposure of acid-induced degradation. So, the three subsets of each mortar type are referred to as Control, Exposed EXT and Exposed INT. The diffractograms for FAGP, in Fig. 6, depict characteristic peaks based on their intensity. Aside from the amorphous phase, which falls between 20° and 30° 2θ, the primary phases available within the FAGP-Control composite are quartz (Q) from sand, mullite (M), and magnetite (N). Mullite ($Al_{5.33}Si_{0.67}O_{9.33}$) indicates the presence of unreacted fly ash particles [46,47]; it is seen at low intensities in the XRD graphs of the FAGP-Exposed EXT zone, confirming a phase transition or ion loss owing to leach-out. Moreover, the development of amorphous sodium aluminosilicate hydrate (N-A-S-H) gel was also observed. This shifted the initial amorphous hump between 15° and 30° and the alumina-silicate glass formation to between 20° and 32°. Furthermore, traces of gypsum can be seen in FAGP-exposed zones (the peak between 10 and 15°), indicating an interaction between sulphuric acid and free accessible Ca^{2+} in low-calcium FA binder. Albite Na(AlSi3O8), Microcline KAlSi3O8, as well as numerous additional unknown phases, in negligible

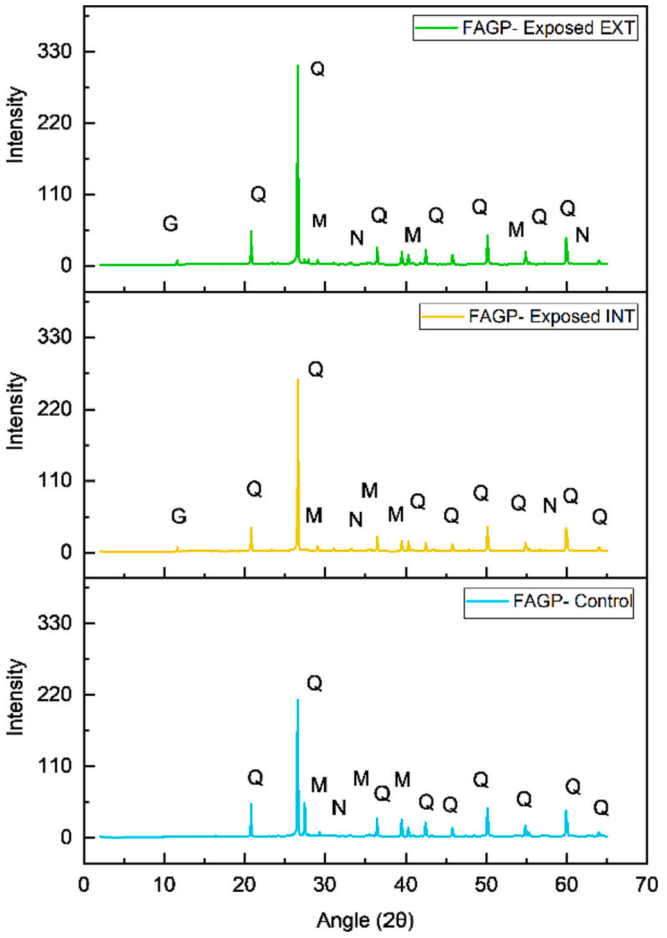

Fig. 6. XRD evolution of FAGP mortar after 30 days of 0.5pH sulphuric acid exposure (quartz (Q) mullite (M), gypsum(G) and magnetite (N)).

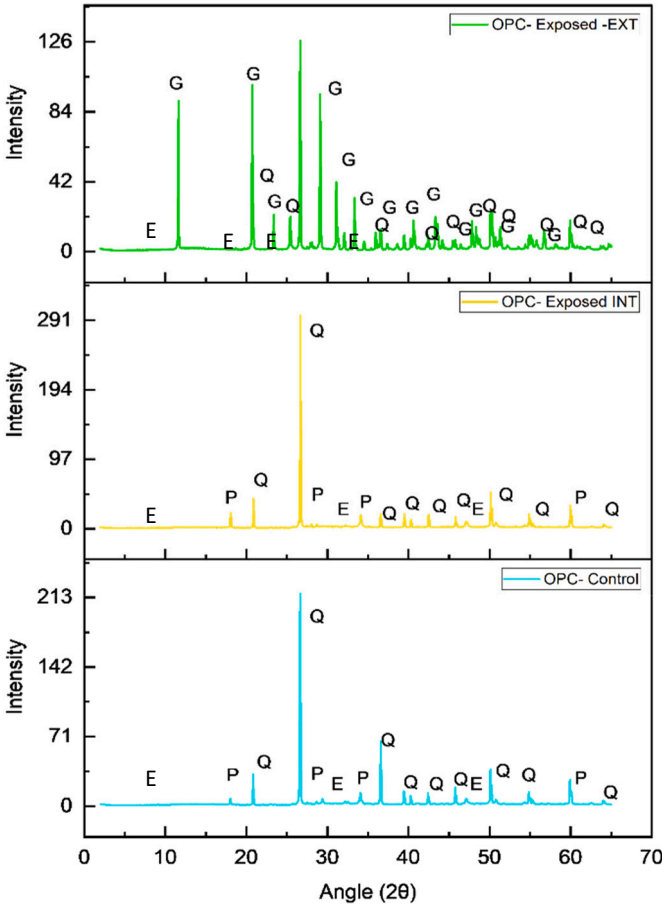

Fig. 7. XRD evolution of OPC mortar after 30 days of 0.5pH sulphuric acid exposure (Q- Quartz, G-Gypsum, *E*-Ettringite and, P- Portlandite).

quantities was found in the acid-exposed FAGP XRD results.

As seen in Fig. 7, there is no discernible difference between the XRD curves for OPC-Control and OPC-INT of the acid-exposed specimen, confirming that the core has yet to encounter acid, thereby preserving its integrity. In contrast, the XRD graph for OPC-Exposed EXT reveals a considerable shift in peak intensities and location compared to unaffected regions; multiple prominent peaks are found at 11.6, 20.7, and 29.1, and these have been identified and reported as gypsum by several studies. This gypsum crystallisation is caused by the decalcification of portlandite in the OPC matrix. Furthermore, minor ettringite peaks can be seen in the OPC-Exposed-EXT zone between 15 and 25, as opposed to the peaks at 9.1, 31.4 and 47.1° in OPC unexposed zones.

3.5. Elemental mapping

Fig. 8 illustrates elemental mappings for FAGP and OPC mortar specimens subjected to sulphuric acid corrosion. Figs. 8(a) and 8(a') show a slice of FAGP and OPC specimens and Figs. 8(b) to 8(e') show the distribution of Ca, Al, S, and Fe ions on the reference surface. As shown in Fig. 8(a), a brown ring is visible in the FAGP specimen at 31 days of sulphuric acid immersion, implying a depth of acid penetration of 5 mm from the specimen's outer surface. The corresponding OPC specimen, in Fig. 8(a'), has a thin white coating with a thin brown layer between it and the sound matrix in the core area.

The Ca profiles for FAGP, and OPC (shown in Fig. 8(b) and 8(b'), respectively) offer an excellent indication of the Ca concentration in each mortar type, which correlate with the XRF data for class F FA used in the mortar. Slight traces of Ca are observed in FAGP, and the calcium concentration is lower in the semi-deteriorated zone, which is the brown ring, than in either the deteriorated or sound matrix of FAGP. However, some arbitrary Ca-rich spots are visible in this region. Compared to FAGP, OPC has dense Ca distribution in the deteriorated outer skin, the semi-deteriorated zone and the sound matrix. The high proportion of Ca in the deteriorated zone is linked to the decalcification of C-S-H in the OPC matrix precipitating as gypsum and ettringite.

The aluminium profile for FAGP, presented in Fig. 8(c), shows that between the deteriorated and sound zones there is a significant difference in concentration. The acid-exposed area exhibits a low-density distribution of Al ions, supporting the possibility of dissolving, which has been widely discussed by Khan et al. [48]. Wang et al. [15] used inductively coupled plasma mass spectrometry to determine the elements leached from the geopolymer paste into the acid solution as part of the sulphuric acid corrosion test. They discovered that the cumulative concentration of Al from the N-A-S-H dominant paste was approximately 38×10^3 ppm at 56-day, which was four-fold the calcium-rich C(N)-A-S-H counterpart. As expected, OPC showed a lower Al^{3+} concentration in the sound matrix (Fig. 8(c')) than in the deteriorated zone of the FAGP specimen. Because of its coagulant characteristics, aluminium ions may have been transported and precipitated at the OPC's deteriorated zone.

In the event of an acid attack, Kiliswa et al. [23] discovered that the mobility of Ca^{2+} is greater than that of Al^{3+}, resulting in a Ca-deficient but aluminium-rich layer that may assist in defending against further acid entry into the sound matrix. This is supported by Pather et al. [40] who reported that the surface layer of FA GPC concrete effectively creates a buffer zone produced by dissolution of alumina hydrate that inhibits acid entry into the internal concrete and retain microstructural integrity. According to Kong et al. [49], the high Al content of the

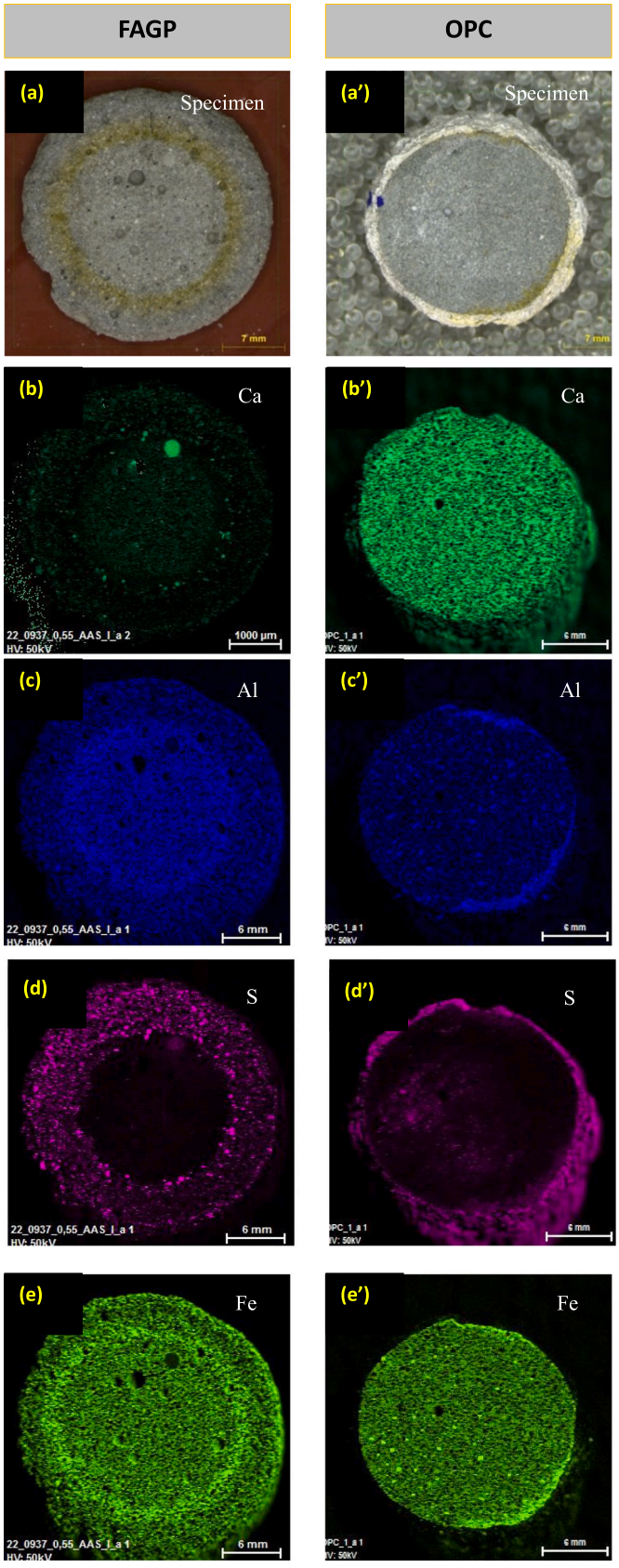

Fig. 8. Comparison of EDS mapping for FAGP and OPC mortars in 0.5 sulphuric acid after 30 days exposure.

geopolymer matrix prevents microbial growth by maintaining the surface pH below between 3 and 4 in sewer conditions.

According to Figs. 8(d) and 8(d'), both FAGP and OPC have a sulphur-free core. FAGP's sulphur-distributed area corresponds to the area including the brown ring, confirming the exposed zone and acid penetration depth. As seen in Fig. 8(d), FAGP sulphur ingress depth is approximately 6 mm, which is slightly higher than the lost wall thickness of the deteriorated OPC. However, the intensity of sulphur distribution in FAGP is lower to the OPC equivalent and is in line with the findings of Khan et al. [48]. The FAGP and OPC matrices reveal an identical ferrous ion distribution in the undeteriorated core (Figs. 8(e) and 8(e')), with the core showing a higher concentration than the deteriorated zone, while ferrous ions can be seen grouped in the semi-deteriorated zone. This might be due to the presence of the reaction product, ferrous sulphate, which is highly soluble in water [50].

3.6. Porosimetry

Porosity is a measurement of the void spaces within a material and is expressed as a percentage of the void volume relative to the total volume. The pore size distribution and connectivity also have critical material properties and performance attributes [51]. Since the combination of these have a linear correlation to density, this governs the performance of solid materials in terms of their mechanical strength, permeability and other macroscopic properties [52,53]. Establishing pore relations and comparing the pore structures of the reference mortar matrix to the acid-exposed mortar can thus be another method for determining the residual integrity level. The MIP technique has been widely used to analyse the pore arrangement of materials, using mercury as the non-wetting fluid that intrudes the pore spaces with external pressure [54,55].

The porosity evolution of representative acid-exposed mortar samples analysed by MIP is shown in Fig. 9. The accumulated pore volume curves are presented in Fig. 9(a) while the deteriorated zone is compared to the undeteriorated interior of the samples for FAGP, OPC and P-GP, respectively in b, c and d. According to Fig. 9(a), acid intrusion has altered porosity in all systems. However, the severity of exposure in terms of pore distribution and change in porosity varies. When subjected to 0.5 pH sulphuric acid at 40 °C, the cumulative pore volumes measured for OPC mortar at the core intact (INT) and the outer deteriorated skin (EXT) were 0.96 and 21.06 mm^3/g, showing a substantial change in pore structure [56]. Among the three mortar types, the unexposed OPC-INT had the lowest share of each pore type: gel pores (dia. < 0.01 μm), capillary pores (0.1 μm < dia. < 1 μm) and macro pores (1 μm < dia.), followed by P-GP-INT. As shown in Fig. 9(b), OPC experienced an enhanced occurrence of capillary pores after acid exposure, which was also confirmed by the microscope pictures (Fig. 3). This is triggered by the reaction of Ca^{2+} with $SO4^{2-}$ which produces porous gypsum. This may let the acid penetrate further into the intact layers of the matrix, leading to highly expansive ettringite formation [29].

The corresponding values of cumulative pore volumes for FAGP mortar were 8.61 and 9.58 mm^3/g, which was one tenth of a pore volume increase and hence inconsequential. It is noted that the FAGP-INT mortar matrix is more porous and less dense than the OPC core (OPC-INT) and this can be attributed to the low amount of CaO and thus a trace of C-A-S-H-like phase [6,10]. This corresponds to the elemental mapping data for sulphur intrusion and aluminium leach out (Figs. 8(c) and 8(d)). FAGP showed a slightly higher acid intrusion depth (<10 %) than OPC (based on OPC's diminished wall thickness caused by acid deterioration). This is due to the porous FAGP matrix, which allows acid to enter through capillary pores. However, sulphur distribution density in FAGP is lower compared to OPC. This is supported by MIP studies. MIP results revealed that the corrosion products had not significantly altered the pore structure because of acid exposure. Unlike in OPC, there is no major shift in the differential pore size distribution curves for FAGP, as seen in Fig. 9(c). This might be due to the overall result of the

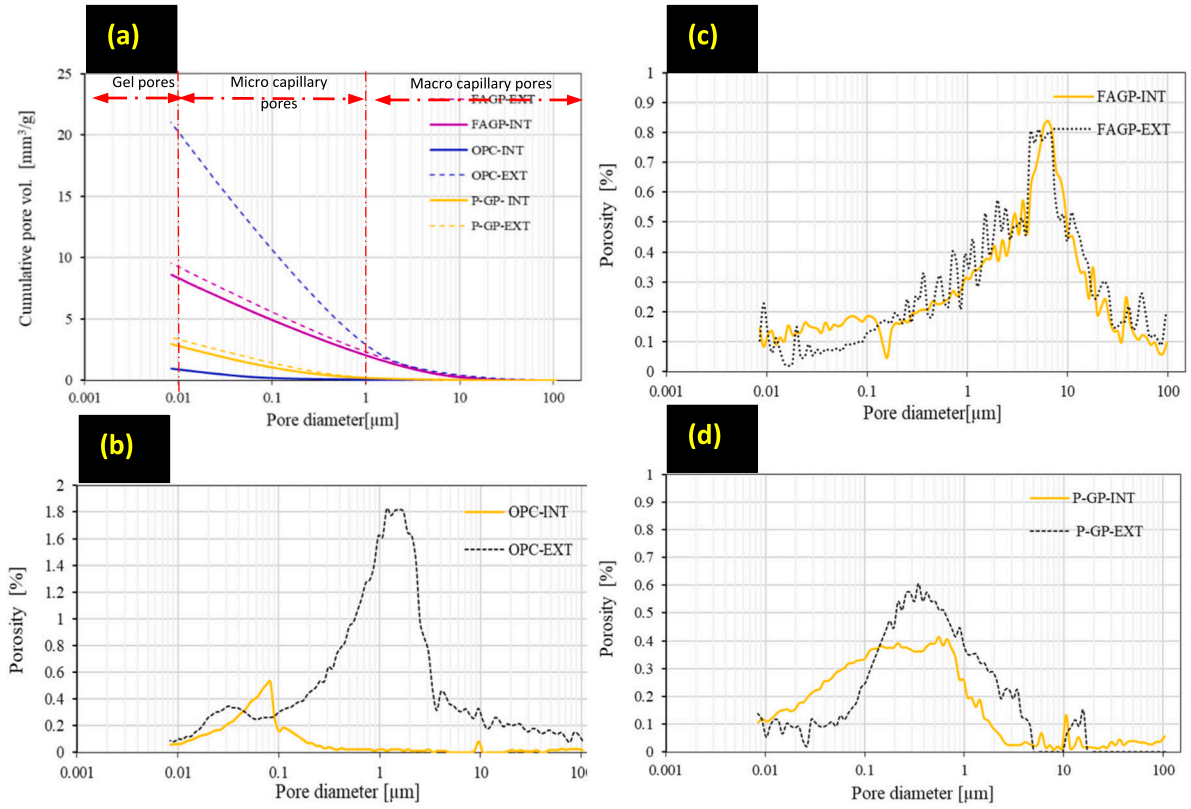

Fig. 9. MIP results for the mortar mixes at the core and deteriorated zone at 30 days of acid exposure (a) cumulative pore volume, (b), (c) and (d) are pore size distribution for OPC, FAGP and P-GP, respectively as a function of pore diameter.

intertwined responses of the hydrates and the inherent microstructure of geopolymer under an acid attack, namely the low calcium content available to react with sulphuric acid and/or the existing pore types in geopolymer due to complicated N-A-S-H gels, which may have impeded acid penetration into the specimen's inner layers [40]. Comparing the core and surface of a commercial geopolymer mortar exposed to sulphuric acid reveals an increase in the proportion of capillary and macro pores, with sizes ranging from 0.1 to 5 μm replacing transitional pores with diameters ranging from 0.01 to 0.1 μm. This may be the cause of the material loss and appears to be exacerbated by the larger aggregates (crushed glass particles) used in the synthesis of P-GP mortar.

According to Fig. 10, the percentages of FAGP and P-GP gel pores are reduced to half due to the harsh sulphuric acid exposure. These pores have either been transformed into larger pores or filled by reaction products, while OPC shows a modest rise. Although there is a comparable percentage of macro pores in the matrix exterior of FAGP and OPC mortars, the micro capillary pores in OPC-EXT are four times greater than in FAGP-EXT. This caused by the corrosion products: expansive gypsum and ettringite. It should be noted for all mortar types that the microcracks formed by cutting the specimens into thin slices may have also contributed to changing pore topologies.

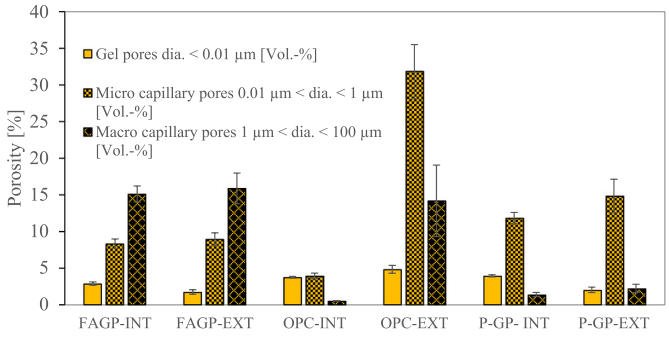

Fig. 10. Comparison of pore size distribution between mortar types.

4. Discussion

The effect of parameters investigated in Fig. 10 and Table 2 were analysed and presented as Stacked bar as the percentage changed in mass, diameter and porosity following acid exposure in Fig. 11. The results of the accelerated corrosion study, where acid-exposed mortars were evaluated using physical, chemical and microstructural criteria, provided an insight into the deterioration mechanism within the mortar types being compared and evaluated.

Fig. 11 clearly indicates that OPC is the most vulnerable mortar to acid-induced sewer corrosion as it suffered significant mass and diameter loss accompanied by an extraordinarily higher percentage of micro and macro pore diameter changes, compared to FAGP and P-GP.

A comprehensive statistical analysis of quantitative data was undertaken in order to confirm the validity of the above visual observation and to establish where there is a statistically significant difference between the mortar types. The percentages of mass loss, diameter loss (Table 2) and change in pore sizes (Fig. 10) were used as dependent variables in the analysis. The results of the analysis of variance (ANOVA) for each parameter are summarised in Table 3. From Table 3, for % Mass loss, the corresponding P-value is 0.001, which is less than the chosen significance level of 0.05, indicating that there is a statistically significant difference between the FAGP and OPC mortar. For all variables, multiple comparisons using the Tukey post hoc procedure indicated a statistically significant difference between FAGP and OPC. However, there was no statistically significant difference between P-GP and FAGP observed except for % Diameter loss.

As is evident from Fig. 11 and Table 3, OPC proved to be very susceptible to aggressive acid exposure. The sulphuric acid exposure

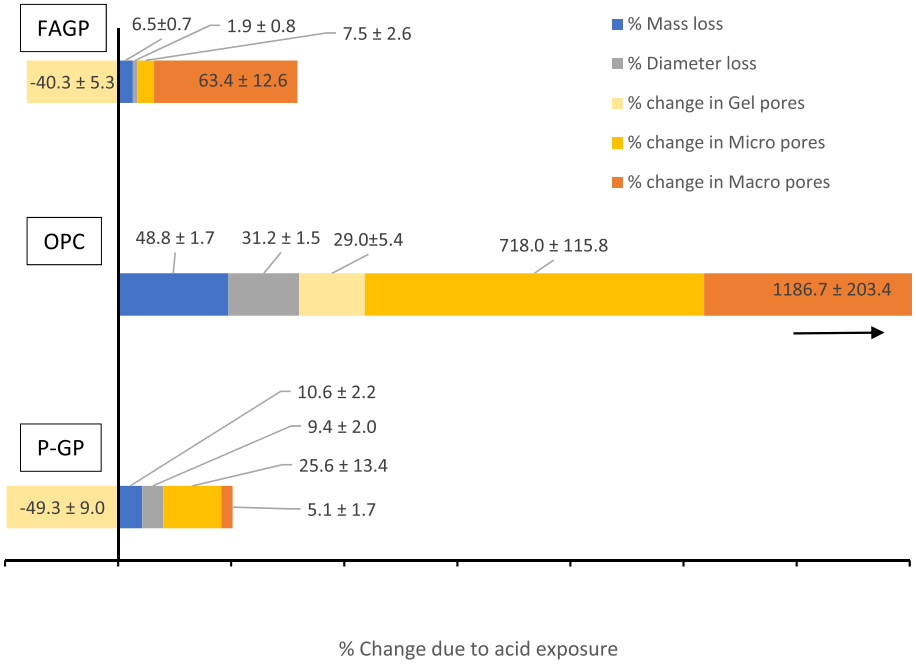

Fig. 11. The percentage changed in mass, diameter and porosity following acid exposure.

Table 3
ANOVA results.

Response		% Mass loss	% Diameter loss	% Change in gel pores	% Change in micro pores	% Change in macro pores
Sum of squares		3264.66	1394.02	11,042.39	984,492.12	2,660,397.01
Mean square		1632.33	697.01	5521.20	492,246.06	1,330,198.50
F-value		485.33	194.15	80.23	72.39	64.046
P-value		<0.001	<0.001	<0.001	<0.001	<0.001
Remarks		Significant	Significant	Significant	Significant	Significant
Tukey HSD - FAGP	OPC	<0.001 Significant	<0.001 Significant	<0.001 Significant	<0.001 Significant	<0.001 Significant
	P-GP	0.075	0.007	0.433	0.961	0.876

changed the pore structure of the OPC by increasing the porosity at macro and micro levels by 718 % and 1187 %, respectively, compared to its initial measurements. The porosimetry results revealed a considerable growth of micro and macro capillary pores at the OPC's deteriorated zone (Fig. 10); the corresponding SEM data (Fig. 4) of the corroded area also verifies this microstructural change. These expanded pores caused macro and micro fissures (Fig. 4) in the matrix. The consequent internal stresses have led to the loss of additional mass while providing a pathway for acid to reach the sound matrix for further reaction. The observed phenomenon can be ascribed to the continual dissolving of Ca^{2+} from the OPC C-S-H gel neutralising the acid, which is confirmed by the pH change data shown in Fig. 1.

The existence of potential corrosion products of this reaction, predominantly expansive gypsum, was confirmed by the qualitative data collected from SEM-EDS analysis (Fig. 3e). Furthermore, the SEM picture of acid-exposed OPC in Fig. 3d indicates the secondary ettringite phase formed by the interaction of gypsum and C-A-S-H bonds in the OPC, which perhaps was involved in developing macro fractures in the OPC degraded zone (Fig. 4a). This suggests that the degradation of sulphuric acid-exposed mortars follows a linear order according to OPC matrix pore evolution and is characterised by the continuing release of slow-releasing cations (Ca^{2+}), resulting in porous corrosion products with high pH neutralising capabilities (Fig. 1).

Fig. 11 shows that the alterations in FAGP and P-GP after acid exposure were minimal compared to OPC. FAGP had mass and diameter losses of just 7 % and 2 %, respectively. These were significantly lower than the OPC counterpart. This is statistically supported by ANOVA results presented in Table 3. The equivalent mass loss and diameter loss for P-GP were 11 % and 9 %, respectively, but were not statistically significant compared to the FAGP values. Both microscopy and mercury intrusion porosimetry data supported this observation. Following acid exposure, FAGP's cumulative pore volume increased (as seen in Fig. 9). This was reflected in the SEM images which show that the extent of particle dispersion in the corroded zone is less intense in FAGP (outside the brown ring in Fig. 5a) than in OPC at the same magnification level. Despite an increase in the micro and macro pores, Fig. 11 illustrates a reduction of gel pores in the FAGP by up to 40 %. This reduction of gel pores can be ascribed to the substitution of micro and macro pores due to ion dissolution from the N-A-S-H links of the FAGP.

The data from variations in solution pH (Fig. 1) corroborate this ion leaching and subsequent ion exchange process, which involved neutralising the sulphuric acid. The EDS mapping results depict the variation in Al and Fe ions concentrations between the core and the deteriorated zone (Fig. 2), suggesting the possible movement of these ions, along with traces of Ca ions, out from the matrix. Another potential explanation for the decrease in FAGP gel pore volume could be the precipitation of corrosion products or modification in the polymeric bonds due to liberated ions following an acid attack. This observation is consistent with FAGP's slower rate of acid neutralisation, as shown in Fig. 2. Compared to the core, the relatively reduced presence of Al ions in the deteriorated zone appears to decrease the effectiveness of acid neutralisation. The percentage of increased micro and macro pores between OPC and FAGP is substantial and statistically significant (Table 3). Nevertheless, P-GP behaved similarly to FAGP regarding the

overall change in the pore structure after acid exposure.

The sulphur mapping for FAGP (Fig. 8(d)) shows evidence of sulphuric acid ingress in the degraded zone. This can be related to the increased micro and macro pores, promoting acid permeation through the deteriorated zone as the dissolution process progresses. However, the sulphur distribution density in FAGP appeared to differ from that of OPC (Fig. 8(d')). This may be attributed to the acid neutralising capacities and distinctive corrosion products and phases that occurred in each mortar following the acid attack. The XRD spectra for OPC Exposed-EXT, depicted in Fig. 6, exhibited prominent gypsum peaks, confirming the substantial presence of sulphur in the degraded zone. However, the OPC-Exposed INT curve (representing the zone at the acid front) showed no signs of gypsum but slight traces of ettringite. This is consistent with the EDS elemental mapping data shown in Fig. 8(d'), where the sulphur distribution of OPC is restricted to the deteriorated zone. The EDS mapping depicts Al ions agglomeration at the OPC's acid front (Fig. 8(c')), which can be ascribed to apparent ettringite formation, as reflected in the XRD discussed above. Consequently, the OPC mass loss can be directly related to the detached material (corrosion products including mortar aggregate) from the degraded zone of the OPC specimen.

Unlike OPC, the gypsum phase in the FAGP corroded zone is low (Fig. 6). This is consistent with the Ca mapping results for FAGP. The insignificant Ca distribution in the degraded zone is attributable to the minimal gypsum production in FAGP following acid exposure, as shown in Fig. 8(b). Hence, it may be inferred that the observed increase in micro and macro pores in FAGP is not primarily attributed to gypsum production. This can be attributed to the formation of non-expansive corrosion products, leachates such as Al (Fig. 8(c)) and Fe (Fig. 8(e)), and their acid neutralising capacity, which differed from the OPC counterpart, resulting in a microstructural alteration with improved acid resistance properties. In summary, low-calcium FAGP stands as the best performing candidate for utilisation as a binder or rehabilitation material in acid-induced sewage corrosion environments as it proved to be more resilient in comparison to OPC, as discussed above.

5. Conclusion

Performance of two mortars (OPC and FAGP) was investigated in this work under accelerated laboratory-induced sewer conditions. The third mortar (P-GP) was used as a reference for mechanical strength and acid resistance properties and was not part of the comparison due to the commercial in confidence nature of the results. A low-calcium FAGP has outperformed the OPC during acid exposure in terms of mass and diameter loss and porosity changes, making it the most suitable candidate for utilisation as a rehabilitation/binder material in such aggressive conditions. Further, qualitative data produced by SEM and XRD not only supported the above findings but also provided insight into the mechanisms attributed to the deterioration. The study's important findings are listed as follows:

- The OPC binder systems showed substantial dissolving of solid material when exposed to sulphuric acid, resulting in severe surface degradation compared to the aluminosilicate geopolymeric counterpart, FAGP.
- The acid neutralisation of FAGP binder appears to be faster than that of OPC binder in the early phases of acid exposure. However, the process is impeded due to insufficient Ca to dissolve.
- Acid-exposed FAGP corrosion phases revealed trace levels of gypsum but no ettringite. The minor mass loss seen in FAGP can be due to ion leach-out from the geopolymer matrix.
- In contrast to OPC binder systems, the proportion of gel pores in geopolymeric binder systems reduced substantially following H_2SO_4 acid exposure. This is attributable to the accumulation of corrosion products or the transformation into larger pores due to dissolving ions from N-A-S-H gels.
- The difference in aluminium concentration between the degraded zone and the sound core of low-calcium geopolymeric binder systems verifies dealumination in hostile acidic conditions. Despite the dissolution of Al, the pore structure appears to have changed minimally. This is attributable to the new geopolymeric gel formed with reoriented Al ions, resulting in a matrix with improved acid resistance.
- The statistical analysis validated the significance of the observed disparities in mass loss, diameter loss and change in porosity between the OPC and low-calcium geopolymeric binder systems following exposure to sulphuric acid. This emphasises that the low-calcium geopolymeric binder systems are a potential candidate for rehabilitation works in aggressive sewer environment.

The shorter experimental duration and the ensuing small sample size might have impaired the accuracy of distinguishing significant relationships within the data sets. Furthermore, the prolonged measurement intervals employed (both before and following exposure) might introduce imperceptible yet substantial phase changes, such as the formation of gypsum and the subsequent pH, microstructural and mass changes. This presents challenges in establishing a correlation between qualitative and quantitative data. Thus, extensive experimental analyses of low-calcium FA geopolymer against sewer conditions in terms of acid consumption and polymeric ion leachate at smaller sampling intervals is recommended. Long-term investigations for the geopolymer degradation in terms of residual mechanical characteristics and severity across close-to-reality sewage conditions are beneficial for predicting service life for each scenario.

CRediT authorship contribution statement

Piumika W. Ariyadasa: Writing – original draft, Methodology, Investigation, Formal analysis, Data curation, Conceptualization. **Allan C. Manalo:** Writing – review & editing, Validation, Supervision, Funding acquisition, Conceptualization. **Weena Lokuge:** Writing – review & editing, Supervision. **Vasantha Aravinthan:** Writing – review & editing, Supervision. **Andreas Gerdes:** Writing – review & editing, Supervision. **Jonas Kaltenbach:** Writing – review & editing, Data curation. **Beatriz Arevalo Galvan:** Writing – review & editing, Data curation.

Declaration of competing interest

The authors declare that they have no known competing financial interests or personal relationships that could have appeared to influence the work reported in this paper.

Data availability

Data will be made available on request.

Appendix A. Supplementary data

Supplementary data to this article can be found online at https://doi.org/10.1016/j.cemconres.2024.107436.

References

[1] V. Athira, et al., Influence of different curing methods on mechanical and durability properties of alkali activated binders, Constr. Build. Mater. 299 (2021) 123963.
[2] M.N.S. Hadi, N.A. Farhan, M.N. Sheikh, Design of geopolymer concrete with GGBFS at ambient curing condition using Taguchi method, Constr. Build. Mater. 140 (2017) 424–431.
[3] T. Gourley, G. Johnson, The Corrosion Resistance of Geopolymer Concrete Sewer Pipe 43 (2019) 38–44.
[4] H. Zhu, et al., Trenchless rehabilitation for concrete pipelines of water infrastructure: a review from the structural perspective, Cem. Concr. Compos. 123 (2021) 104193.

[5] X. Ren, L. Zhang, Experimental study of geopolymer concrete produced from waste concrete, J. Mater. Civ. Eng. 31 (7) (2019) 14.
[6] P. Nuaklong, et al., Properties of high-calcium and low-calcium fly ash combination geopolymer mortar containing recycled aggregate, Heliyon 5 (9) (2019) e02513.
[7] N. Roghanian, N. Banthia, Development of a sustainable coating and repair material to prevent bio-corrosion in concrete sewer and waste-water pipes, Cem. Concr. Compos. 100 (2019) 99–107.
[8] S. John, Y. Nadir, G. K, Effect of Source Materials, Additives on the mechanical properties and durability of Fly ash and Fly ash-slag Geopolymer mortar: a review, Constr. Build. Mater. (2021) 280.
[9] J. Mishra, et al., Sustainable fly ash based geopolymer binders: a review on compressive strength and microstructure properties, Sustainability 14 (22) (2022) 15062.
[10] Q. Fu, et al., The microstructure and durability of fly ash-based geopolymer concrete: a review, Ceram. Int. 47 (21) (2021) 29550–29566.
[11] J.P. Godinho, M.H.F. de Medeiros, Biogenic sulfur attack in a reinforced concrete sewage treatment plant. Re-visited mechanism and rehabilitation proposal, Eng. Fail. Anal. 124 (2021) 105354.
[12] A. Koenig, et al., Resistance of alkali-activated binders to organic acid attack: assessment of evaluation criteria and damage mechanisms, Constr. Build. Mater. 151 (2017) 405–413.
[13] C. Phiangphimai, et al., Durability properties of novel coating material produced by alkali-activated/cement powder, Constr. Build. Mater. 363 (2023) 129837.
[14] M. Wasim, T.D. Ngo, D. Law, A state-of-the-art review on the durability of geopolymer concrete for sustainable structures and infrastructure, Constr. Build. Mater. 291 (2021) 123381.
[15] Y. Wang, et al., Study of acidic degradation of alkali-activated materials using synthetic C-(N)-A-S-H and N-A-S-H gels, Compos. Part B Eng. 230 (2022) 109510.
[16] A. Mehta, R. Siddique, Sulfuric acid resistance of fly ash based geopolymer concrete, Constr. Build. Mater. 146 (2017) 136–143.
[17] H.B. Chang, Y.C. Choi, Accelerated performance evaluation of repair mortars for concrete sewer pipes subjected to sulfuric acid attack, J. Mater. Res. Technol. 9 (6) (2020) 13635–13645.
[18] P.L. Matthieu, et al., An innovative approach to reproduce the biodeterioration of industrial cementitious products in a sewer environment. Part I: test design, Cem. Concr. Res. 73 (2015) 246–256.
[19] W.G. Valencia-Saavedra, R. Mejía de Gutiérrez, F. Puertas, Performance of FA-based geopolymer concretes exposed to acetic and sulfuric acids, Constr. Build. Mater. (2020) 257.
[20] J.P. Gevaudan, B. Santa-Ana, W.V. Srubar III, Iron mineral admixtures improve the sulfuric acid resistance of low-calcium alkali-activated cements, Cem. Concr. Compos. 116 (2021) 103867.
[21] M.P. Lavigne, et al., Innovative approach to simulating the biodeterioration of industrial cementitious products in sewer environment. Part II: validation on CAC and BFSC linings, Cem. Concr. Res. 79 (2016) 409–418.
[22] T.A. Aiken, et al., Effect of slag content and activator dosage on the resistance of fly ash geopolymer binders to sulfuric acid attack, Cem. Concr. Res. 111 (2018) 23–40.
[23] M.W. Kiliswa, K.L. Scrivener, M.G. Alexander, The corrosion rate and microstructure of Portland cement and calcium aluminate cement-based concrete mixtures in outfall sewers: a comparative study, Cem. Concr. Res. 124 (2019) 105818.
[24] C. Grengg, et al., Advances in concrete materials for sewer systems affected by microbial induced concrete corrosion: a review, Water Res. 134 (2018) 341–352.
[25] H.A. Ali, et al., Enhancing the resistance to microbial induced corrosion of alkali-activated glass powder/GGBS mortars by calcium aluminate cement, Constr. Build. Mater. 341 (2022) 127912.
[26] A. Darabnoush, Z. Kohankar, M. Najafi, A framework for structural design of geopolymer spray applied pipe lining, in: Pipelines 2011, 2011, pp. 55–65.
[27] J. Matthews, J. Royer, Laboratory Testing and Analysis of Geopolymer Pipe-lining Technology for the Rehabilitation of Sewer and Stormwater Conduits, 2019.
[28] J. Zhang, et al., Durability of alkali-activated materials in aggressive environments: a review on recent studies, Constr. Build. Mater. 152 (2017) 598–613.
[29] H.A. Khan, et al., Deterioration of alkali-activated mortars exposed to natural aggressive sewer environment, Constr. Build. Mater. 186 (2018) 577–597.
[30] H. Ye, L. Huang, Degradation mechanisms of alkali-activated binders in sulfuric acid: the role of calcium and aluminum availability, Constr. Build. Mater. 246 (2020) 118477.
[31] P. Zhang, et al., A review on properties of fresh and hardened geopolymer mortar, Compos. Part B Eng. 152 (2018) 79–95.
[32] W. Lokuge, et al., Design of fly ash geopolymer concrete mix proportions using multivariate adaptive regression spline model, Constr. Build. Mater. 166 (2018) 472–481.
[33] P. Sajan, et al., Combined effect of curing temperature, curing period and alkaline concentration on the mechanical properties of fly ash-based geopolymer, Cleaner Materials 1 (2021) 100002.
[34] T. Wells, R.E. Melchers, An observation-based model for corrosion of concrete sewers under aggressive conditions, Cem. Concr. Res. 61-62 (2014) 1–10.
[35] S. Madraszewski, et al., Experimentally driven evaluation methods of concrete sewers biodeterioration on laboratory-scale: a critical review, Constr. Build. Mater. 320 (2022) 126236.
[36] K. Chen, et al., Geopolymer concrete durability subjected to aggressive environments–a review of influence factors and comparison with ordinary Portland cement, Constr. Build. Mater. 279 (2021) 122496.
[37] C. Grengg, et al., Long-term in situ performance of geopolymer, calcium aluminate and Portland cement-based materials exposed to microbially induced acid corrosion, Cem. Concr. Res. 131 (2020) 106034.
[38] T. Wells, R.E. Melchers, Modelling concrete deterioration in sewers using theory and field observations, Cem. Concr. Res. 77 (2015) 82–96.
[39] H.A. Khan, et al., Durability of calcium aluminate and sulphate resistant Portland cement based mortars in aggressive sewer environment and sulphuric acid, Cem. Concr. Res. 124 (2019) 105852.
[40] B. Pather, S. Ekolu, H. Quainoo, Effects of aggregate types on acid corrosion attack upon fly–ash geopolymer and Portland cement concretes–comparative study, Constr. Build. Mater. 313 (2021) 125468.
[41] A. Allahverdi, F. Škvára, Acidic corrosion of hydrated cement based materials. Part 1. Mechanism of the phenomenon, Ceramics-Silikáty 44 (2000) 114–120.
[42] J. Monteny, et al., Chemical and microbiological tests to simulate sulfuric acid corrosion of polymer-modified concrete, Cem. Concr. Res. 31 (9) (2001) 1359–1365.
[43] M. Albitar, et al., Durability evaluation of geopolymer and conventional concretes, Constr. Build. Mater. 136 (2017) 374–385.
[44] H.A. Khan, A. Castel, M.S.H. Khan, Corrosion investigation of fly ash based geopolymer mortar in natural sewer environment and sulphuric acid solution, Corros. Sci. 168 (2020).
[45] Z. Li, et al., Corrosion behaviour and mechanism of basalt fibres in acidic and alkaline environments, Corros. Sci. 110 (2016) 15–22.
[46] F. Puertas, et al., A model for the C-A-S-H gel formed in alkali-activated slag cements, J. Eur. Ceram. Soc. 31 (12) (2011) 2043–2056.
[47] A. Fernández-Jiménez, A. Palomo, Characterisation of fly ashes. Potential reactivity as alkaline cements☆, Fuel 82 (18) (2003) 2259–2265.
[48] H.A. Khan, M. Yasir, A. Castel, Performance of cementitious and alkali-activated mortars exposed to laboratory simulated microbially induced corrosion test, Cem. Concr. Compos. 128 (2022) 104445.
[49] L.J. Kong, et al., Application potential of alkali-activated concrete for antimicrobial induced corrosion: a review, Constr. Build. Mater. 317 (2022).
[50] F.K. Cameron, The solubility of ferrous Sulphate, J. Phys. Chem. 34 (4) (1930) 692–710.
[51] H. Ma, Mercury intrusion porosimetry in concrete technology: tips in measurement, pore structure parameter acquisition and application, J. Porous. Mater. 21 (2) (2014) 207–215.
[52] Z. Zhu, et al., Correlations between unconfined compressive strength, sorptivity and pore structures for geopolymer based on SEM and MIP measurements, Journal of Building Engineering 67 (2023) 106011.
[53] R. Abousnina, et al., Characteristics, strength development and microstructure of cement mortar containing oil-contaminated sand, Constr. Build. Mater. 252 (2020) 119155.
[54] C.M. Tibbetts, et al., Mercury intrusion porosimetry parameters for use in concrete penetrability qualification using the Katz-Thompson relationship, Constr. Build. Mater. 263 (2020) 119834.
[55] C. Ng, et al., A review on microstructural study and compressive strength of geopolymer mortar, paste and concrete, Constr. Build. Mater. 186 (2018) 550–576.
[56] L. Kong, et al., Mechanism study of the role of biofilm played in sewage corrosion of mortar, Constr. Build. Mater. 164 (2018) 44–56.